

# Vortices in atomic-molecular Bose-Einstein condensates

Tristram J. Alexander<sup>1</sup>, Yuri S. Kivshar<sup>1</sup>, Elena A. Ostrovskaya<sup>1</sup>, and Paul S. Julienne<sup>2</sup>

<sup>1</sup>*Nonlinear Physics Group, Research School of Physical Sciences and Engineering, The Australian National University, Canberra ACT 0200, Australia*

<sup>2</sup>*Atomic Physics Division, National Institute of Standards and Technology, Gaithersburg, MD 20889*

The structure and stability of vortices in hybrid atomic-molecular Bose-Einstein condensates is analyzed in the framework of a two-component Gross-Pitaevskii-type model that describes the stimulated Raman-induced photoassociation process. New types of topological vortex states are predicted to exist in the coherently coupled two-component condensates even without a trap, and their nontrivial dynamics in the presence of losses is demonstrated.

PACS numbers: 03.75.Fi, 03.65.Ge, 05.30.Jp, 32.80.Pj

## I. INTRODUCTION

Recent experimental observation of the photoassociation of Bose condensed atoms via the stimulated Raman process and the production of ultracold molecules [1] is, undoubtedly, the first step towards the creation of a coherently coupled atomic-molecular condensate. Such a system would represent a rich ground for exploring a variety of the nonlinear atom-optics effects, analogous to those known for the processes of parametric up and down conversion of light waves [2,3]. From this point of view, the excited topological states of the macroscopic wavefunction—*vortices*—in the atomic-molecular Bose-Einstein condensates are of great interest as a direct counterpart of the parametric vortices in nonlinear optics [4,5]. On the other hand, the study of such topological states is important for understanding the properties of composite superfluids, such as the recently proposed molecular Bose-Einstein condensate (BEC) coupled to a cloud of Fermi atoms [6], or the composite atomic-molecular BEC (AMBEC) [7].

From the experimental point of view, it is important to not only establish the conditions for the formation of topological states, but also identify the states which are dynamically stable, i.e. are not destroyed by exponentially growing collective excitations of the condensate. One of the proposed methods for the observation of vortices involves imaging of the expanding condensate released from a trap, with a vortex core growing during the expansion. The atomic-molecular condensate represents an interesting experimental challenge as the excited states may be formed in a dynamically stable, self-confined droplet [7], after the hybrid condensate is released from a trap.

Assuming further experimental progress towards the creation of the molecular and hybrid atomic-molecular BECs, in this paper we analyse the dynamics of the parametrically coupled atomic and molecular condensates, in the framework of a two-component mean-field model [8] that takes into account all types of the mean-field atomic and molecular interactions [7]. For the first time to our knowledge, we study the structure, stability, and dynam-

ics of topological states in AMBEC, and, in particular, we reveal that the dynamically stable *two-component vortex solitons* can be formed in both trapped and untrapped AMBEC clouds. Unlike the conventional vortices predicted and already observed in atomic BEC, vortex solitons can exist as stable *self-trapped states* even without a trapping potential, supported by an *effectively attractive interaction* between the parametrically coupled atomic and molecular components.

Another crucial problem is the dynamics of AMBEC and its topological states in the presence of dissipation, i.e. loss of atoms and molecules from the corresponding fractions of the hybrid BEC. The formation of BEC in the presence of losses due to either a coherent Raman photoassociation process or Feshbach resonance has been analyzed previously [9,10], however the dissipative dynamics of vortices, earlier studied for a single-component atomic BEC [11,12], has never been discussed in the context of hybrid condensates.

Since, so far, no conclusive experimental data are available that would allow us to estimate the rates of the condensate losses rigorously, in this work we take them into account by including *the phenomenological dissipative terms*, and then considering the dissipation rates for which the topological states can still be formed. We analyze the dynamics of the vortex solitons in the presence of dissipation and reveal that they can exhibit a nontrivial decay scenario, with the decay rates much smaller than the characteristic loss rates. Since the physical principles underlying the existence and stability of these topological states are rather generic, we expect that the similar structures can be found in more realistic models of the atomic-molecular BEC dynamics, and eventually observed in experiment.

## II. MODEL

We study the dynamics of the hybrid atom-molecular condensates, produced by a coherent stimulated Raman photoassociation process in a strongly anisotropic trap with a tight confinement along one spatial dimension.

We model the parametrically interacting condensates by a system of two coupled Gross-Pitaevskii (GP) equations for the macroscopic wave functions of the atomic ( $\Psi_a$ ) and molecular ( $\Psi_m$ ) components (see details and references, e.g., in Ref. [7]):

$$\begin{aligned} i\frac{\partial\Psi_a}{\partial t} + \frac{1}{2}\Delta\Psi_a - V_a\Psi_a - \chi\Psi_a^*\Psi_me^{i\delta t} \\ - (U_{aa}|\Psi_a|^2 + U_{am}|\Psi_m|^2)\Psi_a = iR_a, \\ i\frac{\partial\Psi_m}{\partial t} + \frac{1}{4}\Delta\Psi_m - V_m\Psi_m - \frac{1}{2}\chi\Psi_a^2e^{-i\delta t} \\ - (U_{mm}|\Psi_m|^2 + U_{am}|\Psi_a|^2)\Psi_m = iR_m, \end{aligned} \quad (1)$$

where the wave functions, time, and spatial coordinates are measured in the units of  $x_0^{-3/2}$ ,  $\omega_\perp^{-1}$ , and  $x_0 \equiv (\hbar/m\omega_\perp)^{1/2}$ , respectively. Here  $\omega_\perp$  is the characteristic frequency in the plane  $(x, y)$  of the weak confinement of the trap for the atomic BEC fraction. Consequently,  $V_a = (1/2)r^2 + (\lambda^2/2)z^2$  and  $V_m = r^2 + \lambda^2z^2$ , with  $r^2 = x^2 + y^2$ , and  $\lambda^2 = \omega_z/\omega_\perp \gg 1$ . In these notations, the interaction strengths  $U_{ij}$  are measured in the units of  $(\hbar\omega_\perp)^{-1}x_0^{-3}$ , and the Raman-induced coupling,  $\chi$ , in the units of  $(\hbar\omega_\perp)^{-1}x_0^{-3/2}$ . The terms  $R_{a,m}$  on the right hand side are the phenomenological loss terms which will be discussed and specified below in Sec. 4.2.

Due to significantly dissimilar scales of spatial confinement in the different directions, and the *quasi-two-dimensional* geometry of the trap, the form of the condensate wavefunction in the  $z$  direction is completely determined by the structure of the harmonic trap. We therefore assume that the wavefunction can be factorized in the following way:  $\Psi_{a,m} = \phi_{a,m}(x, y, t)\Phi_{a,m}(z)$ , where  $\Phi_{a,m}(z)$  satisfy the one-dimensional harmonic oscillator equations:

$$\frac{1}{2}\frac{\partial^2\Phi_{a,m}}{\partial z^2} - v_{a,m}(z)\Phi_{a,m} + \epsilon_{a,m}\Phi_a = 0, \quad (2)$$

where  $v_a = (1/2)\lambda^2z^2$  and  $v_m = 2\lambda^2z^2$ . The ground state solutions of these equations correspond to  $\epsilon_a = \lambda/2$  and  $\epsilon_m = \lambda$ , so that  $\Phi_a = C_a \exp(-\lambda z/2)$  and  $\Phi_m = C_m \exp(-\lambda z)$ . The normalization conditions  $\int \Phi_{a,m}^2 = 1$  yield  $C_a = (\lambda/\pi)^{1/4}$  and  $C_m = (2\lambda/\pi)^{1/4}$ .

Substituting the factorized wavefunctions into the model equations, multiplying the first and second equations by  $\Phi_a$  and  $\Phi_m$ , respectively, integrating to eliminate the  $z$  dependence, and introducing  $\psi_{a,m}(x, y, t) = \phi_{a,m}(x, y, t) \exp(-i\lambda t/2)$ , we obtain the final evolution equations for the wavefunctions of a ‘‘pancake’’-shape AMBEC:

$$\begin{aligned} i\frac{\partial\psi_a}{\partial t} + \frac{1}{2}\Delta_\perp\psi_a - V_a(r)\psi_a - \tilde{\chi}\psi_a^*\psi_me^{i\delta t} \\ - \left(\tilde{U}_{aa}|\psi_a|^2 + \tilde{U}_{am}|\psi_m|^2\right)\psi_a = i\tilde{R}_a, \\ i\frac{\partial\psi_m}{\partial t} + \frac{1}{4}\Delta_\perp\psi_m - V_m(r)\psi_m - \frac{1}{2}\tilde{\chi}\psi_a^2e^{-i\delta t} \\ - \left(\tilde{U}_{mm}|\psi_m|^2 + \tilde{U}_{am}|\psi_a|^2\right)\psi_m = i\tilde{R}_m, \end{aligned} \quad (3)$$

where  $\Delta_\perp = \partial^2/\partial x^2 + \partial^2/\partial y^2$ ,  $V_a(r) = (1/2)r^2$ , and  $V_m(r) = r^2$ . Here we introduce the renormalized interaction strengths:  $\tilde{U}_{aa} = U_{aa}(\lambda/2\pi)^{1/2}$ ,  $\tilde{U}_{mm} = U_{mm}(\lambda/\pi)^{1/2}$ ,  $\tilde{U}_{am} = U_{am}(2\lambda/3\pi)^{1/2}$ ,  $\tilde{\chi} = \chi(\lambda/2\pi)^{1/4}$  and, correspondingly, the renormalized loss terms  $\tilde{R}_{a,m}$ . For the sake of clarity, we omit the tilde from the equations throughout the following text. One can see that the renormalization factors absorbed by the interaction coefficients as a result of the reduction to the 2D geometry are, in fact, close to 1 for typical  $\lambda \sim 10$ .

For definiteness, we consider the case of  $^{87}\text{Rb}$ , for which the production of ultracold molecules were recently demonstrated experimentally [1], and assume that the Raman detuning parameter vanishes,  $\delta = 0$ . Using the recently reported data for the intra- and inter-species scattering lengths [1], we take  $U_{aa} = 0.062$ ;  $U_{am} = -0.084(\pm 0.07)$ , and  $\chi = 1.09$ . The large uncertainty in the value of  $U_{am}$  corresponds to the s-wave scattering length,  $a_{am} = -180a_0 \pm 150a_0$ , recently measured experimentally [1]. Since the molecular BEC has not been experimentally realized yet, the exact value of  $U_{mm}$  is not known, although it can be estimated to be of the order of the other interaction strengths (see details in Ref. [7]) and, therefore, it cannot be ignored in the model (3).

It has also been previously established that the qualitative behaviour of the system depends on the sign of the determinant  $\Delta U \equiv U_{aa}U_{mm} - U_{am}^2$  [7,8], which defines the relative strength of the cubic interactions. Parameter  $U_{mm}$  can therefore be used to investigate the system in two distinct regimes of the net *attractive*  $\Delta U > 0$  and net *repulsive*  $\Delta U < 0$  cubic interactions [7]. At the low particle numbers, i.e. for the low densities of the condensate wavefunctions, and in the parameter region where  $\Delta U \approx 0$ , the interactions are dominated by the parametric, i.e. quadratic, coupling ( $\sim \chi$ ) which can be *effectively attractive or repulsive*, depending on the relative phase of the molecular and atomic components [7]. The structure and dynamical properties of all topological structures in the AMBEC is controlled by the complex interplay of the quadratic and cubic inter- and intra-component mean-field interactions.

### III. VORTEX SOLITONS

Spatially localized ground-state solutions of the model (3) at  $R_a = R_m = 0$ , with and without the trapping potential  $V_j(r)$ , have been analyzed earlier [7]. Here, we are interested in the excited states of the model (3) that correspond to the topological vortex states of the hybrid two-component condensate. In order to find the vortex states, we consider the model equations (3) *without the dissipative terms* (i.e.  $R_a = R_m = 0$ ), and look for the radially symmetric solutions with a nontrivial phase in the form:

$$\begin{aligned}\psi_a(r, \theta, t) &= \phi_a(r) e^{ik_a \theta - i\mu_a t}, \\ \psi_m(r, \theta, t) &= \phi_m(r) e^{ik_m \theta - i\mu_m t},\end{aligned}\quad (4)$$

where  $(r, \theta)$  are the polar coordinates in the plane of the trap, and  $\mu_{a,m}$  are the chemical potentials of the corresponding AMBEC fractions. Due to the parametric coupling between the atomic and molecular matter waves, the existence of *stationary states* of the AMBEC requires the phase-matching conditions,  $\mu_m = 2\mu_a \equiv 2\mu$ , and  $k_m = 2k_a \equiv 2n$ , so that the integer  $n$  defines the topological charge of the AMBEC vortex soliton via its atomic component.

The spatially localized, radially symmetric solutions of the model (3) in the form (4) can be found by a standard numerical relaxation technique. Different types of such topological states are summarized in Fig. 1 for the case  $n = 1$  (single-charged vortices). The upper solid curve in the middle part of Fig. 1 [that includes the point (d)] corresponds to *stable vortices in a trapping potential*; such vortices are supported by the effectively *repulsive cubic interaction* since  $\Delta U < 0$ . These topological states are somewhat similar to the vortices of a single-component atomic BEC, and they expand when released from the trap. At the low particle numbers [see the inset in Fig. 1, dashed curve with the point (c)], these vortex solutions become unstable due to the competition between the effectively *attractive quadratic* and *repulsive cubic* interaction. Thus, the repulsive nature of the inter-species cubic interaction manifests itself only for large densities of the components  $\phi_a$  and  $\phi_m$ .

Thick solid curve in Fig. 1 (and the insert) describes a family of the vortices of the single-component *purely molecular* condensate wavefunction  $\psi_m$  [see the case (a)], whereas a dotted curve above it corresponds to another family of *hybrid vortices* that bifurcates from the purely molecular states. This second family of the two-component vortices is supported by an effectively *repulsive quadratic* nonlinearity allowing such states to exist for low particle numbers but only in the presence of a trapping potential [cf. an example in (b)].

An important feature of the model (3) is the existence of untrapped self-localized *vortex solitons* for  $\mu < 0$ . These structures are supported by an effectively *attractive quadratic* interaction between the atomic and molecular components. As the parameter  $\mu$  decreases, the solution becomes broader due to the presence of effectively repulsive cubic nonlinearity, with a saturation amplitude of the wavefunction corresponding to the amplitude of the spatially homogeneous (free-space) condensate wavefunction [see the cases (e) and (f) in Fig. 1].

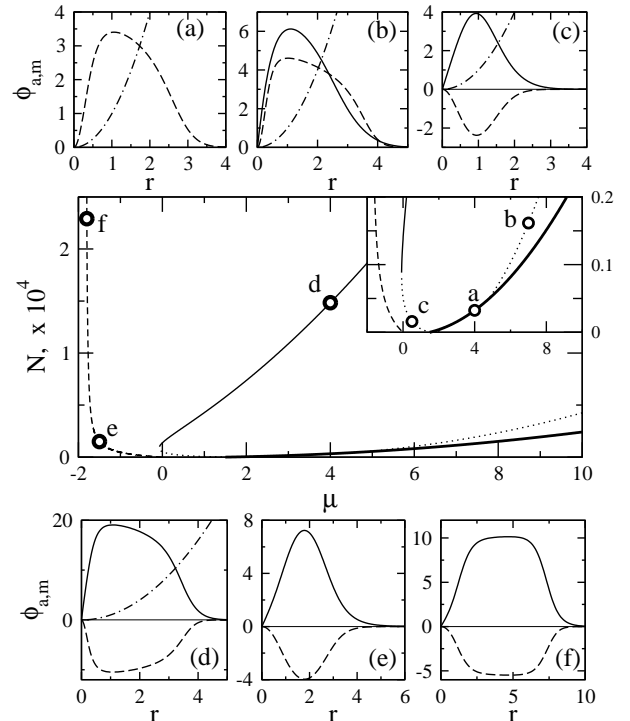


FIG. 1. Middle: Different families of the stationary one- and two-component vortex states in the model (3). Thin solid/dashed - stable/unstable hybrid vortices in a trap, dotted - unstable vortices in a trap, dashed - untrapped self-localized vortex solitons. Thick solid - vortices of a molecular condensate. Top and bottom: Examples of the stationary profiles of the vortices corresponding to the marked points. Dashed-dotted curves in (a)-(d) show the trapping potential. Insert: Close-up of the bifurcation region.

In this paper, we determine the vortex stability by a direct numerical propagation, but a more rigorous stability analysis will be presented elsewhere. We find that the broad vortex solitons [shown, e.g., in Fig. 1(f)] are *stable*, whereas narrow vortex solitons [e.g. those shown in Fig. 1(e)] are *unstable*, in agreement with the earlier analysis of the parametric vortices in optics [5]. Interestingly, for the unstable vortices we observe two types of the instability-induced dynamics, i.e. the break-up into *two* or *three* filaments, for larger and smaller particle numbers, respectively. This dynamical behaviour is a clear signature of the transition between the regime of effectively cubic interaction in which the vortex soliton decays into  $2|n|$  filaments [13], and the regime of effectively quadratic interaction when the vortex soliton breaks up into  $2|n| + 1$  filaments, as usually observed for quadratic parametric beams [14].

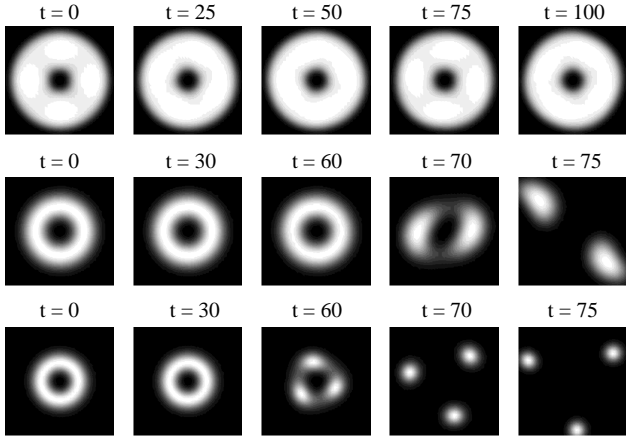


FIG. 2. Lossless dynamics of the self-trapped vortex soliton. Top: stable propagation of a broad vortex, the case (f) in Fig. 1 ( $\mu = -1.8$ ). Middle: the symmetry-breaking instability induced by the effective cubic nonlinearity,  $\mu = -1.5$ , the case (e) in Fig. 1. Bottom: the symmetry-breaking instability induced by parametric interaction,  $\mu = -0.5$ . Only the atomic component is shown.

## IV. DISSIPATION-INDUCED VORTEX DYNAMICS

### A. Physical estimates of the losses

In the formation of ultracold molecules from an atomic BEC, the processes of the incoherent production of molecules, decays of the atomic excited state, and inelastic collisions between atoms and molecules, all contribute to the effective loss of particles from the corresponding fractions of the BEC, resulting in the dissipative dynamics of the localized AMBEC states.

To take into account all possible losses in the hybrid condensate, we introduce the following linear and nonlinear (i.e., density-dependent) dissipative terms into the GP model (3),

$$\begin{aligned} R_a &= -\nu_a \psi_a - \gamma_a |\psi_a|^2 \psi_a - \gamma_{am} |\psi_m|^2 \psi_a, \\ R_m &= -\nu_m \psi_m - \gamma_m |\psi_m|^2 \psi_m - \gamma_{am} |\psi_a|^2 \psi_m, \end{aligned} \quad (5)$$

where the dimensionless coefficients,  $\nu_j$  and  $\gamma_j$ , stand for the decay rates of the atomic excited state ( $\sim \nu_a$ ) and the excited molecules into high bound states of the atomic BEC or “hot” (non-BEC) atoms ( $\sim \nu_m$ ), the rates of inelastic collisions and decay of the atomic states ( $\sim \gamma_a$ ), and inelastic molecule-molecule collisions and dissociation into high bound state or continuum state of the molecular BEC ( $\sim \gamma_m$ ), and atom-molecule inelastic collisions resulting in the production of “hot” atoms and molecules ( $\sim \gamma_{am}$ ).

The linear loss terms in Eq. (5) are similar to those discussed earlier in Ref. [9], however the latter work did not take into account the losses due to the rotationally or

vibrationally inelastic atom-molecule collisions, as well as the molecule-molecule collision losses. System (3) with the loss terms (5) is formally equivalent to the mathematical description of the formation of AMBEC through Feshbach resonances [10], except for the terms responsible for the linear losses from the excited atomic state ( $\sim \nu_i$ ) which are specific for the AMBEC production via the coherent Raman photoassociation process. We stress that no conclusive experimental data for the losses that would enable the coherent AMBEC production are available at the moment, so some reasonable estimates need to be made.

In Eqs. (5), the coefficients for the collisional losses,  $\gamma_j$ , are measured the units of  $\Gamma = x_0^3 \omega_\perp$ , and for the typical values of  $x_0 \sim 5 \mu\text{m}$ , and  $\omega_\perp \sim 10^2 \text{ Hz}$ ,  $\Gamma \sim 10^{-8} \text{ cm}^3/\text{s}$ . In what follows, we investigate the effect of relatively “weak”,  $\gamma_j = 10^{-3}$  and “strong”,  $\gamma_j = 10^{-1}$  losses, which nevertheless corresponds to physically “strong” inelastic collisions rates of  $\Gamma = 10^{-11} - 10^{-9} \text{ cm}^3/\text{s}$ . For simplicity, we assume that all the inelastic loss rates in the model are equal to each other.

As was estimated in Ref. [9], the linear loss rates that still enable the coherent dynamics of the AMBEC are of the order of  $10^2 \text{ s}^{-1}$ , which corresponds to our dimensionless values of  $\nu_j \sim 1$ . Assuming this to be the case, we note that the term responsible for the “weakest” nonlinear losses in our model still an order of magnitude larger than the corresponding linear loss, i.e.  $\Gamma n_j \sim 10^3 \text{ s}^{-1}$  for the typical condensate density of  $n_j \sim 10^{14} \text{ cm}^{-3}$ . This means that, without loss of generality, we can assume that  $\gamma_j = \nu_j$  in our model, and bear in mind that the effect of the linear losses is only significant when the particle numbers (and condensate densities) are small.

The other (strong) loss mechanism for the molecular fraction, which is absent in our effectively two-mode consideration, is the coupling of a molecule to the other, excited states of the atomic BEC due to the closeness of the excited molecular level to the BEC atom-pair level. This loss channel has been recently shown to be responsible for the enhancement of the condensate loss rates [15]. One can argue, however, that on the time scales large compared with the corresponding rates of decay into the higher-order modes, the lowest-order nonlinear excited modes of the hybrid AMBEC that we consider here become decoupled from the rest of the bound state spectrum, and all losses associated with such coupling can be effectively incorporated into the phenomenological terms proportional to  $\nu_m$ .

### B. Lossy dynamics of the vortex soliton

In the presence of losses, the total particle number in both components of AMBEC decreases. First of all, when the molecular component is small, the effective equations (3) can be decoupled and the dissipative dynamics of two

components can be described separately. In particular, neglecting the molecular component, and averaging over the spatial structure of the atomic BEC wavefunction, from Eqs. (3),(5) we obtain the simple equation for the density  $n_a = |\psi_a|^2$  of the atomic component

$$i \frac{dn_a}{dt} = -2\nu_a n_a - 2\gamma_a n_a^2, \quad (6)$$

which has the analytic solution,

$$n_a(t) = \frac{\nu_a e^{-2\nu_a t}}{(C - \gamma_a e^{-2\nu_a t})}, \quad (7)$$

where  $C = \gamma_a + \nu_a/n_a(0)$ . When the effect of linear losses can be neglected, the decay of the atomic component follows a power law.

We have conducted the numerical simulations of the dissipation-induced dynamics of the vortex soliton varying the loss terms. In Fig. 3, we show the decay of the maximum amplitude of the atomic component  $n_a^{\max} = |\psi_a|_{\max}^2$  of the two-component vortex soliton in the presence of the losses of a different strength. For “strong” and “medium” losses ( $\gamma = \nu = 0.1$  and  $0.01$  respectively), the decay follows approximately the analytical dependence (7) and, therefore, the modal (spatial) structure of the vortex state is not very important.

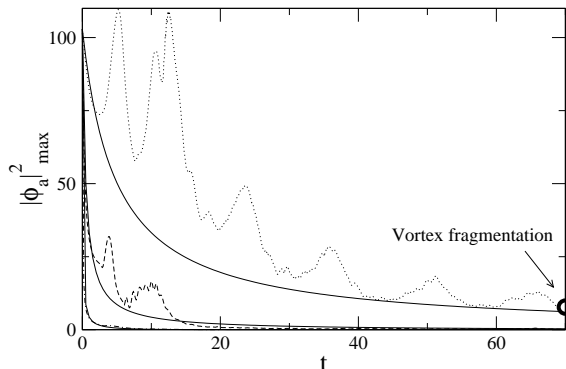


FIG. 3. Decay of the atomic component amplitude for different values of losses. The initial state is a self-trapped vortex soliton as in Fig. 1(f) and Fig. 2(top). Losses are: 0.001 (dotted), 0.01 (dashed), and 0.1 (dash-dotted). Thin solid lines show the analytic dependence (7).

For weaker losses, we reveal novel features in the vortex dynamics associated with the interplay between the instability-induced vortex fragmentation and the decay of the vortex amplitude due to losses. As an example, in Fig. 4(top) we show the propagation of the initially stable, untrapped, vortex soliton [shown as (f) in Fig. 1] in the presence of weak dissipation,  $\gamma_i = \nu_i = 0.001$ . While this vortex is absolutely stable in the lossless regime (see Fig. 2, top), its number of particles decreases and the corresponding vortex solution moves along the dashed curve in Fig. 1 from the point (f) to the point (e), entering the lower part of the branch corresponding to unstable vortices. Then, the vortex fragmentation into two or three

filaments occurs, as shown in Fig. 4(top). This leads us to conclude that the fragmentation to components occurs when the particle number has dropped far enough to place the vortex in the region of instability for stationary solutions and, overall, the vortex parameters adiabatically follow the family of untrapped localized solutions.

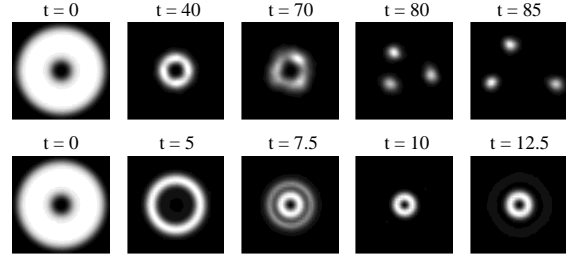


FIG. 4. Dynamics of the (initially) stable vortex soliton in the presence of losses: (a) weak,  $\gamma_i = \nu_i = 0.001$ , and (b) strong,  $\gamma_i = \nu_i = 0.01$ .

For comparison, in Fig. 4(bottom) we show the vortex dynamics for stronger losses, when no fragmentation is observed at all. In this case, the vortex soliton does not follow a family of localized solutions adiabatically. Moreover, it appears that the dissipation leads to a switching from the fundamental vortex state to one of the higher-order vortex modes. The additional “rings” in the density distribution observed in Fig. 4 (bottom) therefore seem to be a manifestation of such a higher-order mode.

### C. Evolution of a vortex released from a trap

Although different possibilities to create the topological states in experiment may exist, it is probably safe to assume that the presence of the confining trap is paramount. The question therefore is whether a dynamically stable topological state of AMBEC created in a trap can be transformed into a dynamically stable vortex in a self-confined AMBEC droplet, after the hybrid condensate is released from the trap. We investigate such a possibility by conducting additional numerical studies.

A trapped vortex, corresponding to the stable family shown in the main part of Fig. 1 [the branch that includes the point (d)] is released from the trap at  $t = 0$ . We find that for weak or no dissipation this vortex structure diffracts rapidly, as shown in Fig. 5(top). However, when the losses become large enough, the released vortex state gets *self-trapped*, as shown in Fig. 5(bottom).

In order to verify the effect of self-trapping and get a deeper insight into our results, we use the parametric plot of the system Hamiltonian  $H(t)$  vs. the total particle number  $N(t)$ , which both evolve in time in the presence of losses. For weak losses, we reveal that the vortex dynamics follows the “trapped” family of the vortex states (dashed line in Fig. 6). The family of the trapped vor-

text states in this plot corresponds to the initial conditions of a trapped vortex stationary solution with the trapping potential turned off. This vortex state diffracts when it is released from the trap due to the dominant repulsive cubic nonlinearity. However, for stronger losses we observe a novel effect when the vortex, being initially released from the trap, does not rapidly diffract but, instead, it switches to a self-trapped vortex soliton, as shown by a dotted curve in Fig. 6.

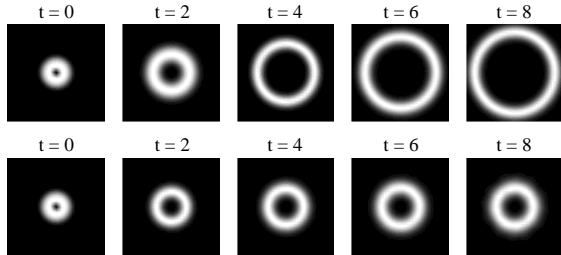


FIG. 5. Dynamics of a vortex state formed in a trap and released from the trap at  $t = 0$ , under the influence of (a) weak ( $\gamma = \nu = 0.001$ ) and (b) strong ( $\gamma = \nu = 0.01$ ) losses.

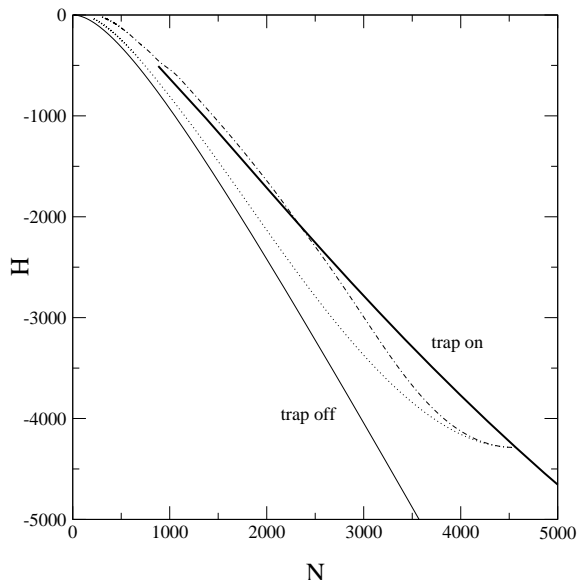


FIG. 6. Parametric plot  $H(t)$  vs.  $N(t)$  for the vortex evolution shown in Fig. 5. Solid (thick and thin) lines - the families of the vortex states with and without the trap, respectively. Dashed and dotted curves show the dynamics of the stable vortex initially formed in a trap and released from it in the presence of losses,  $\gamma = \nu = 0.001$  and  $\gamma = \nu = 0.01$ , respectively.

## V. CONCLUSIONS

In the framework of a two-component mean-field model of hybrid coherently coupled condensates, we have analyzed the structure, stability, and dynamics of the topological states in the atomic-molecular BEC created via

the induced two-color Raman photoassociation process. We have predicted the existence of novel two-component vortex solitons supported by the coherent parametric coupling between the atomic and molecular BEC fractions, and demonstrated that such topological states can exist even in the absence of a trapping potential.

Since the losses are known to be very important in the formation of the hybrid atomic-molecular condensates, we have analyzed the effect of weak and strong losses of a different physical origin on the dynamics of the vortex solitons, the type of problems never addressed in other fields such as nonlinear optics. In particular, for the first time to our knowledge, we have described an interplay between the nonlinearity-induced vortex fragmentation and dissipation-induced vortex decay. Moreover, we have revealed that the losses may be very useful to identify the self-trapped vortex states in the hybrid condensates in experiment, after releasing the atomic-molecular condensate from a trap.

Although our analysis is valid for a quasi-two-dimensional model, the generalization to a spherically symmetric case seems straightforward. Additionally, in spite of the limited validity of the two-component model, we believe that the similar types of topological states can be found in more realistic models of hybrid condensates, as well as in other types of coherently coupled mixtures of the multi-component condensates such as spinor Bose-Einstein condensates.

The work has been supported by the Planning and Performance Fund of the Institute of Advanced Studies at the Australian National University.

- 
- [1] R. Wynar *et al.*, *Science* **287**, 1016 (2000); see also B. Goss Levi, *Physics Today*, September 2000, pp. 46-50.
  - [2] P.D. Drummond, *Mod. Phys. Lett. B* **14**, 189 (2000).
  - [3] U.V. Poulsen and K. Molmer, *Phys. Rev. A* **63**, 023604 (2001).
  - [4] T.J. Alexander *et al.*, *Phys. Rev. E* **61**, 2042 (2000).
  - [5] I. Towers *et al.*, *Phys. Rev. E* **63**, 055601(R) (2001).
  - [6] E. Timmermans, K. Furuya, D.W. Milonni, and A. K. Kerman, *Phys. Lett. A* **285**, 228 (2001).
  - [7] B.J. Cusack *et al.*, *Phys. Rev. A* (2001) in press.
  - [8] see, e.g., E. Timmermans, *et al.*, *Phys. Rep.* **315**, 199 (1999), and references therein.
  - [9] D.J. Heinzen *et al.*, *Phys. Rev. Lett.* **84**, 5029 (2000).
  - [10] V.A. Yurovsky, A. Ben-Reuven, P.S. Julienne, and C. J. Williams, *Phys. Rev. A* **62**, 043605 (2000).
  - [11] P.O. Fedichev, and G.V. Shlyapnikov, arXiv:cond-matt/9902204 (1999).
  - [12] B. Jackson, J.F. McCann, and C. S. Adams, *Phys. Rev. A* **61**, 013604 (2000).
  - [13] W.J. Firth and D.V. Skryabin, *Phys. Rev. Lett.* **79**, 2450 (1997).

- [14] J.P. Torres, J.M. Soto-Crespo, L. Torner, and D.V. Petrov, *J. Opt. Soc. Am. B* **15**, 625 (1998); D.V. Skryabin and W.J. Firth, *Phys. Rev. E* **58**, 3916 (1998); G. Molina-Terriza, S. Minardi, A. Bramati, P. Di Trapani, and L. Torner, *Opt. Express* **9**, 110 (2001).
- [15] V. A. Yurovsky, A. Ben-Reuven, and P.S. Julienne, *arXiv:cond-mat/0108372* (2001).